Neutron charge radius determined from the energy dependence of the neutron transmission of liquid ^{208}Pb and ^{209}Bi

S. Kopecky,[1] J. A. Harvey,[2] N. W. Hill,[2] M. Krenn,[1] M. Pernicka,[3] P. Riehs,[1] and S. Steiner[1,*]
[1]*Institut für Kernphysik der Technischen Universität Wien, A-1020 Vienna, Austria*
[2]*Oak Ridge National Laboratory, Oak Ridge, Tennessee 37831*
[3]*Institut für Hochenergiephysik, Nickolsdorfergasse 6, A-1060 Vienna, Austria*
(Received 2 May 1997)

The ORELA experiment on the neutron charge radius has been reevaluated. The neutron transmission of liquid thorogenic ^{208}Pb with the neutron time-of-flight method in the neutron energy range from 0.08 to 800 eV was measured. Additional studies on condensed matter effects for liquid Bi and liquid Pb have provided more accurate corrections resulting in smaller systematic uncertainties for the neutron-electron scattering length b_{ne}. We have also reevaluated the transmission data on liquid Bi of Melkonian and co-workers. We have obtained values of $b_{ne}=(-1.33\pm0.027\pm0.03)\times10^{-3}$ fm for ^{208}Pb and $b_{ne}=(-1.44\pm0.033\pm0.06)\times10^{-3}$ fm for ^{209}Bi where for both results the two uncertainties denote the statistical and the systematic uncertainty, respectively. The results for ^{208}Pb and ^{209}Bi were found to be in good agreement. [S0556-2813(97)02610-1]

PACS number(s): 14.20.Dh, 25.40.Dn, 32.80.Cy

I. INTRODUCTION

The charge radius of the neutron $\langle r_n^2\rangle$ or the mean squared charge radius is described by the volume integral over the neutron $\int\rho(r)r^2d\tau$, where r is the distance to the center of the neutron and $\rho(r)$ is the charge density. Positive as well as negative values of $\rho(r)$ will occur coming from the distributions of valence quarks and the negative π-meson cloud outside. Since $\rho(r)$ is negative for larger r values, caused by the meson cloud, the r^2 dependence of the integral will lead to a negative value of $\langle r_n^2\rangle$.

Many experiments have been carried out to determine $\langle r_n^2\rangle$. In the literature the neutron-electron scattering length b_{ne} is usually measured and is related to the charge radius $\langle r_n^2\rangle$ by

$$\langle r_n^2\rangle=\frac{3m_e a_0}{m_n}b_{ne}, \tag{1}$$

where a_0 denotes the Bohr radius and m_n and m_e are masses of neutron and electron mass, respectively.

For ^{208}Pb and ^{209}Bi, the most suitable elements for determining b_{ne} from transmission measurements, the elastic scattering is dominated by coherent neutron waves of the neutron nucleus interaction. The cross section is about 10 b and is described in first order by $\sigma_{\rm coh}=4\pi b_c^2$ where b_c is the coherent scattering length which does not depend on neutron energy.

The effect of neutron-electron scattering is caused by the interaction of the charge radius $\langle r_n^2\rangle$ with the electric charge densities of nucleus and electrons bound in diamagnetic atoms. Neutron waves scattered by the nuclear interaction and those scattered by the charge density interfere coherently with each other.

Thus the neutron-electron cross section σ_{ne} is expressed in first order by the interference term [1]

$$\sigma_{ne}=-4\pi\{2b_c b_{ne}[Z-f(Z,E)]\}, \tag{2}$$

where σ_{ne} is always positive since b_{ne} is negative because of the inherent structure of the neutron. The charge density of an atom is given by $Z-f(Z,E)$, where $f(Z,E)$ takes into account the electron cloud and is obtained from a 4π integration over the atomic form factor $f(Z,q)$ which is measured by x-ray scattering [2]. Figure 1 shows $Z-f(Z,E)$ for lead atoms and determines with Eq. (2) the energy dependence of σ_{ne}. For sufficient low energies E the contribution from $Z-f(Z,E)$ is negligible and $\sigma_{ne}=0.0$ b. For sufficient

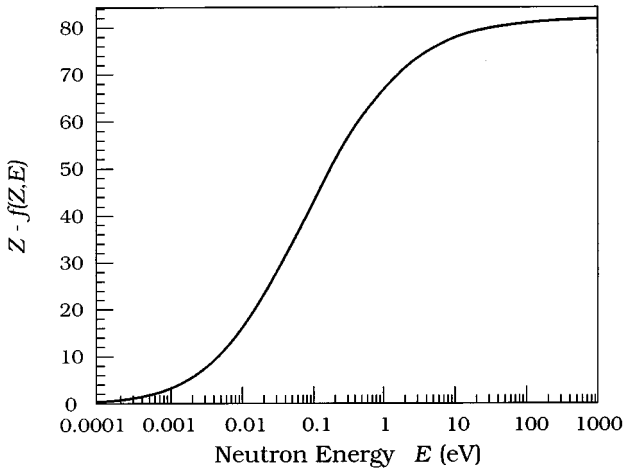

FIG. 1. Illustration of $Z-f(Z,E)$, the atomic charge density of Pb for neutron energies E between 10^{-4} and 10^3 eV.

*Permanent address: Physik Institut der Universität Zürich, Winterthurerstrasse 190, CH-8057 Zürich, Switzerland

TABLE I. Experimental results of b_{ne} in units of 10^{-3} fm.

Experiment	Target	Result	Reference
Angular scattering	Ar	-0.1 ± 1.8	1947 [7] Fermi
Transmission	Bi	-1.9 ± 0.4	1951 [8] Havens
Angular scattering	Kr, Xe	-1.5 ± 0.4	1952 [9] Hamermesh
Mirror reflection	Bi/O	-1.39 ± 0.13	1953 [10] Hughes
Angular scattering	Kr, Xe	-1.4 ± 0.3	1956 [11] Crouch
Crystal spectrometer transmission	Bi	-1.56 ± 0.05	1959 [2] Melkonian
		-1.49 ± 0.05	1976 in Ref. [15]
		$-1.44\pm0.033\pm0.06$	1997 this work
Angular scattering	Ne, Ar, Kr, Xe	-1.34 ± 0.03	1966 [12] Krohn
Angular scattering	Ne, Ar, Kr, Xe	-1.30 ± 0.03	1973 [13] Krohn
Single crystal scattering	^{186}W	-1.60 ± 0.05	1975 [14] Alexandrov
Filter-transmission, mirror reflection	Pb	-1.364 ± 0.025	1976 [15] Koester
Filter-transmission, mirror reflection	Bi	-1.393 ± 0.025	1976 [15] Koester
n-TOF transmission, mirror reflection Ref. [17]	Bi	-1.55 ± 0.11	1986 [16] Alexandrov
Filter-transmission, mirror reflection	Pb, Bi	-1.32 ± 0.04	1986 [17] Koester
n-TOF transmission	thorogenic ^{208}Pb	$-1.31\pm0.03\pm0.04$	1995 [1] Kopecky
		$-1.33\pm0.027\pm0.03$	1997 this work
Filter-transmission, mirror reflection	Pb-isotopes, Bi	-1.32 ± 0.03	1995 [5] Koester
Garching-Argonne compilation	[12,13,15,17]	-1.31 ± 0.03	1986 [3] Sears
Dubna compilation	[14,16]	-1.59 ± 0.04	1989 [19] Alexandrov
Foldy approximation, b_F		-1.468	1952 [18] Foldy

high energies we obtain $Z-f(Z,E)=Z$ and $\sigma_{ne}=-4\pi[2b_c b_{ne}Z]\simeq 0.2$ b, whereas the strong interaction remains almost unchanged over the whole energy range. Therefore, it is evident that $\simeq 95\%$ of the change of neutron-electron cross section occurs in the range from zero up to 18 eV [3].

In the literature, see Table I, some important knowledge for b_{ne} has been deduced with the help of Eq. (2). Information for Eq. (2) is obtained from accurate measurements of the transmission $T(E)$ of neutrons through a sample given by

$$T(E)=\exp[-N\sigma_{\rm tot}(E)], \tag{3}$$

where N is the sample thickness. Here we have $\sigma_{\rm tot}=\sigma_{\rm coh}+\sigma_{ne}$ if we assume for the moment that no other cross sections are contributing.

Recently, we carried out careful investigations where $T(E)$ has been measured for liquid thorogenic ^{208}Pb with the neutron time-of-flight (TOF) method. Finally, we obtained with the ^{208}Pb data [4], a set of eight very good single runs. Figure 2 shows the results of one run in the energy range between 0.08 and 10.0 eV.

Also plotted are four data points for liquid ^{209}Bi which came from one of 10 runs listed in the Tables III and IV. These ^{209}Bi data were measured by Melkonian *et al.* [5] four decades ago: Monochrome reactor neutrons were supplied with a crystal spectrometer. The total cross sections as well as the corrections were published [5]. This allowed to calculate $T(E)$ for Eq. (3). For the plot values of Bi we assumed a thickness of $N=0.187$ atoms/b which is equivalent to our Pb scattering thickness.

The measurement and evaluation of the ^{208}Pb data are the basis of the present publication. We describe the neutron TOF measurement for the ^{208}Pb data (Sec. III) as well as the data analysis (Sec. IV) where a refined calculation of the condensed matter correction (Sec. IV C) produced a small change of our previous result of b_{ne}.

Furthermore, we have reevaluated the ^{209}Bi data [5] since the original result from these data disagreed with our value [4], see Table I. We tried to find the reason for this disagreement [6] and analyzed the transmission data of Refs. [4] and [5] with the same evaluation technique.

II. LITERATURE

As early as 1947 Fermi and Marshall [7] realized the coherent interference between neutrons scattered by the nucleus and the atomic cloud and made the first attempt to measure b_{ne}.

A chronological listing of the experimental results [3–5,7–17] is given in Table I showing a variety of methods. Besides the angular correlation experiment of Krohn and

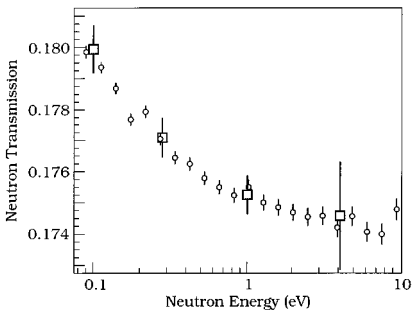

FIG. 2. (○) transmission of one run of the ^{208}Pb data [4] and (□) transmission of one set of the ^{209}Bi data [5].

Ringo [12,13], highest accuracies are correlated to the high precision of the transmission method. However, the experiments of this paper (the ^{208}Pb data and ^{209}Bi data) are the only accurate ones relying only on the transmission method as a function of the neutron energy E. The other accurate transmission experiments [15–17] needed for a sufficient sensitivity of b_{ne} a very good knowledge of b_c from mirror reflection at low energies.

The first theoretical estimation of the neutron-electron interaction was derived by Foldy [18] in 1952. He considered the interaction of a pointlike neutron with an external electromagnetic field. The main contribution, arising from the anomalous magnetic moment of the neutron, corresponds to the Foldy-scattering length $b_F = -1.468 \times 10^{-3}$ fm. As shown in Table I the value of b_F accounts for approximately 90% of the total neutron-electron scattering length. Therefore, there cannot be any doubt that the neutron-electron scattering length has a negative sign.

In recent years, the reliability of experimental values of b_{ne} has been discussed extensively [19–26]. The main attention has been laid on the fact that the experiments can be grouped around two values, which differ by approximately 20% or about five standard deviations. In addition it has been emphasized that b_{ne}-b_F shows different signs for the two groups. New interesting experimental [27] as well as basic physics aspects [28] indicate that the discussion will be continued in the future.

III. MEASUREMENT

The measurements of the ^{208}Pb data were performed at the Oak Ridge electron linear accelerator ORELA. The neutron TOF source had a repetition rate of 100 Hz and a pulse width of 20 ns. Transmission data were taken at a flight path length of 18 m in the energy range between 0.07 eV and 10 keV.

The neutron detection system consisted of a 1 mm ^{6}Li-glass scintillator and two RCA 8854 photomultiplier tubes. The tubes were mounted perpendicular to the incoming neutron beam, viewing the scintillator from both sides. The analog signals of the two tubes were added and fed into a 100 Mhz flash analog-to-digital converter (ADC) providing a continuous 256 channel bit pattern. The scintillator timing signal generates bit patterns in the flash ADC coming from the neutron time of flight (TOF) as well as from the pulse height of the detector signal. With the TOF data and the pulse height data a two-dimensional histogram is populated and stored on disk and magnetic tape. For each run histograms were taken for open beam, sample in the beam, various filters in the beam, etc., and are considered to be the raw data of the experiment.

Figure 3 shows an example of the neutron-TOF spectra where the spectra were normalized and converted to neutron energy. The insert of Fig. 3 gives a pulse height spectrum dominated by neutron events as seen by the (n,α) peak of ^{6}Li. To carry out a high accuracy transmission measurement it is essential to control in detail the spectrum of the detector signal pulse height for both the ''open beam'' and the ''sample in beam'' as a function of neutron TOF to insure that the photomultipliers and their gates perform correctly (the photomultiplier gates suppress the effects of the prompt

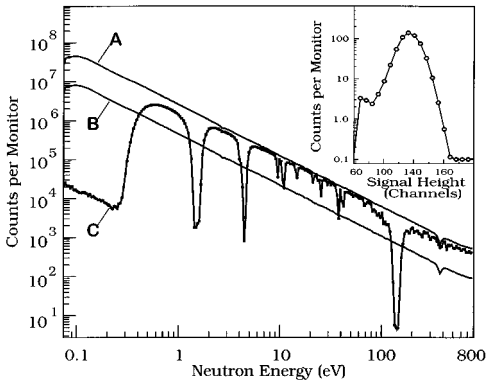

FIG. 3. Sums of raw data for open beam (curve A), liquid ^{208}Pb sample in the beam (curve B), and open beam with filters of Cd, Co, and In (curve C). The insert shows a pulse height distribution of the ^{6}Li peak from the detector.

γ flash to a high degree). The discrimination was checked by the sharp cut off at low channel numbers and by the channel position of the ^{6}Li peak. Finally, a computer made diagram for the time differences between subsequent pulses allowed to see quantitatively any deviations from the requested exponential distribution.

In addition any neutrons can be identified at the bottom of ''blacking out'' resonances or at the Cd cutoff as shown in curve C of Fig. 3. For the detector setup of flight path No. 1 at 18 m only very few neutrons were observed at the bottom of blacking out resonances.

The deadtime of the whole data-acquisition system was $\simeq$130 ns and gave corrections below 1%. Since we recorded the time differences between two subsequent signals, we were able to handle this correction with an accuracy which is more than sufficient for our purpose. The neutron overlap was reduced with a 0.7 mm Gd foil. The remaining overlap was measured using a repetition rate of 50 Hz, enabling us to correct accurately for this effect. To determine the background we used both polyethylene scatterers and black resonance filters. A very good consistency was achieved for the main transmission (deduced by curves A and B in Fig. 3) after correcting for the attenuation of neutrons and γ rays through scatterers and filters. The signal-to-background ratio in the black resonances was as high as 1500. The applied corrections for deadtime, overlap and background are shown in Fig. 1 of Ref. [4].

Because of the required high sensitivity for small cross section changes, we needed low transmission values $T(E)$ and therefore thick condensed matter samples, see Eq. (3). As it is very difficult to correct for interference effects of any solid material, liquid materials are to be preferred (see Fig. 5, curve C) and we started the measurements with samples of natural liquid lead (see Fig. 4). All samples had a diameter of 5 cm and a length of 5 cm. Both ends of the cylinder were closed with Al windows which had a thickness of 3.5 mm. Two thermoelements were inserted into the lead sample to measure the temperature of the heating coils as well as of the liquid directly. For the ''open beam'' position two Al plates compensate the Al-windows of the sample holder. The ''open beam'' plates were heated with a separate heating device. This was necessary to avoid some spurious effects. They were observed for different temperatures of the sample

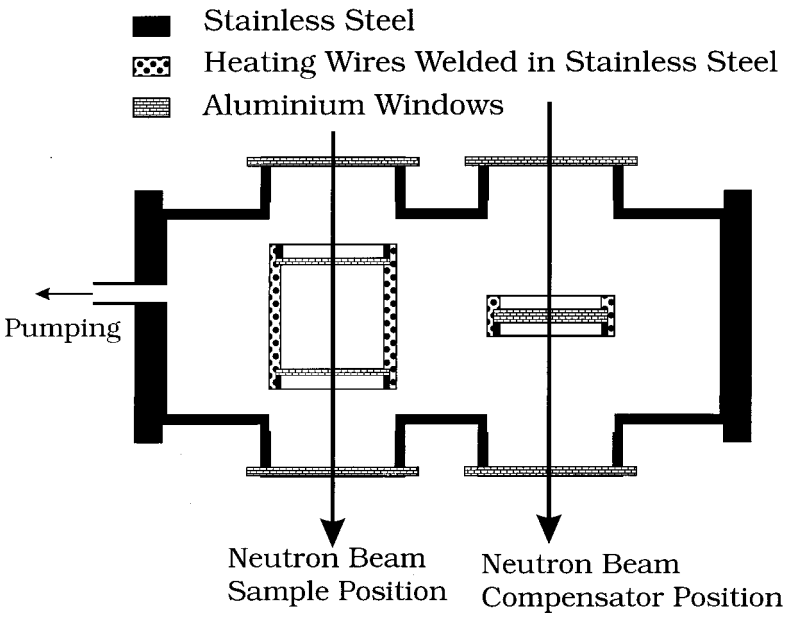

FIG. 4. Cylindrical shaped vacuum container with heating coils for the thorogenic ^{208}Pb sample as well as for the Al disks in the open beam simulating the sample windows.

windows and the compensator plates in a previous experiment at very low energies.

Later on we continued with a thorogenic lead sample which had a thickness of 0.154 atoms/b and finally, we obtained with this sample the set of eight runs of the ^{208}Pb data which were measured at a sample temperature of 623.16 K. The isotopic composition was 0.5% ^{204}Pb, 25.82% ^{206}Pb, 1.65% ^{207}Pb, and 72.54% ^{208}Pb. The abundance of ^{207}Pb is much lower than that one for the natural lead. Therefore and contrary to the natural lead both the absorption and the incoherent scattering of the sample are small enough to be known with sufficient accuracy (see Fig. 5, curve D). In addition the less critical energy dependence of the resonance correction is much smaller (see Fig. 5, curve I).

IV. DATA ANALYSES

A. Neutron cross sections

The total cross section $\sigma_{\rm tot}(E)$ for Eq. (3) is given as a function of the neutron energy E by

$$\sigma_{\rm tot}(E)=\sigma_{\rm coh}(E)S_{\rm coh}(E)+\sigma_{\rm inc}(E)S_{\rm inc}(E)+\sigma_{\rm abs}(E), \tag{4}$$

where $\sigma_{\rm abs}$, $\sigma_{\rm coh}$, and $\sigma_{\rm inc}$ are the absorption, coherent scattering, and incoherent scattering cross section, respectively. The functions $S_{\rm coh}(E)$ and $S_{\rm inc}(E)$ describe the condensed matter correction.

For the nuclides and the energy range of concern the absorption cross section shows a $1/v$ behavior. Therefore we write for the cross section

$$\sigma_{\rm abs}(E)=\frac{c_{\rm abs}}{\sqrt{E}}, \tag{5}$$

where the constant $c_{\rm abs}$ is determined from the cross section data of Ref. [29].

For the incoherent cross section $\sigma_{\rm inc}$ we have to consider two contributions accounting for the variation of the scattering lengths: the spin and the isotopic incoherence. The cross section can be written as

$$\sigma_{\rm inc}=\sum_{j,k}\sum_{s,s'} p_j p_k g_{js} g_{ks'}(a_{js}-a_{ks'})^2. \tag{6}$$

The sums extend over all isotopes j,k and the possible spin orientations s,s' where p_j, p_k are the abundances of the isotopes and $g_{js}, g_{ks'}$ the spin statistical factors of the isotopes

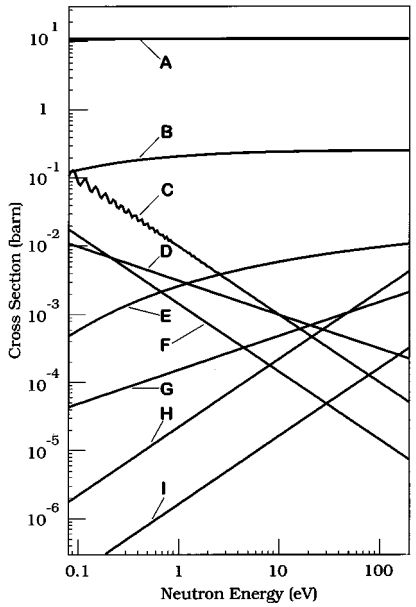

FIG. 5. The cross section of our ^{208}Pb sample $\sigma_{\rm coh}(E)$ is shown in curve A as a sum of the contributions B to I. Curve B: + effect by b_{ne} as given in Eq. (2), curve C: − interference correction, curve D: + absorption, curve E: + Schwinger scattering, curve F: + Doppler effect, curve G: + polarizability, curve H: − effective range effect, curve I: − (resonance correction + 0.1 mb).

and spin states. Finally $a_{js}, a_{ks'}$ are the scattering lengths for the respective spin state of the isotopes.

The expression for the coherent scattering cross section is in first Born approximation

$$\sigma_{\rm coh}=4\pi\{b_c(E)+b_R(E)-b_{ne}[Z-f(Z,E)]+b_p(E)\}^2 + \sigma_{\rm LS}(E), \tag{7}$$

where $\sigma_{\rm LS}(E)$ denotes the Schwinger cross section, $b_c(E)$ the nucleus coherent scattering length [30] including the effective range correction, $b_R(E)$ the energy dependent contribution of the resonance scattering [29] and $b_p(E)$ the contribution caused by the polarizability of the neutron [31].

B. Evaluation procedure

The important interference term of Eq. (2) which is sensitive to values of b_{ne} can be found in Eq. (7). Furthermore, Eqs. (3)–(7) contain all relevant quantities. Most of them are described in more detail in the following Secs. IV C, IV D, and IV E. Altogether, Eqs. (3)–(7) determine the procedure to obtain values of b_{ne} from the data.

First we calculate the transmission data $T(E)$ as a function of E. For the ^{208}Pb data the $T(E)$ values are obtained from the raw data correcting for deadtime, background, and overlap neutrons. For the ^{209}Bi data we obtain the $T(E)$ values from the published cross sections (Ref. [5] in Table I) and from the corrections (Ref. [5] in Table III).

Then, with Eqs. (4)–(7), the calculations were carried out to fit b_{ne} with the method of least squares. Because of the relative high uncertainties of the absolute values of $T(E)$, we fit the relative transmission as a function of the neutron energy E using a normalization factor. Hence, we have a two-parameter fit with (i) b_{ne} and (ii) the normalization as fit parameters. The normalization factor is not noted in the equations.

C. Corrections

The Schwinger cross section is the cross section of the neutron spin-orbit coupling and can be written according to Ref. [1] as

$$\sigma_{\rm LS}=S\sigma_F \tag{8}$$

in which $\sigma_F=4\pi b_F^2$ is the Foldy cross section and

$$S=\frac{1}{2k^2}\int_0^{2k}[Z-f(Z,q)]^2\left[\left(\frac{2k}{q}\right)^2-1\right]q\,dq. \tag{9}$$

In this equation q is given by the momentum transfer $\hbar k$, where k denotes the wave number $k=2.1968\times10^{-4}\sqrt{E}[m_A/(m_A+m_n)]$ (k in fm^{-1} and E in eV). The quantity m_A is the atomic mass and the function $f(Z,q)$ is the differential atomic form factor which is also responsible for the integrated form factor $f(Z,E)$ mentioned earlier. The values of $\sigma_{\rm LS}$ are shown in Fig. 5, curve E.

The scattering length $b_p(q)$ of the electric polarizability of the neutron can be approximated with the nuclear charge radius $R_N=1.2027A^{1/3}$ fm by

$$b_p(q)=\alpha_n Z^2\frac{e^2m}{\hbar^2}\frac{1}{R_N}g(q) \tag{10}$$

with

$$g(q)=\left[\frac{6}{5}-\frac{1}{4}\pi qR_N+\frac{1}{7}(qR_N)^2-\frac{1}{540}(qR_N)^4+\cdots\right], \tag{11}$$

where the constant α_n is the electric polarizability [31] (see Fig. 5, curve G).

The resonance scattering length $b_R(E)$ for the resonance contribution is given in terms of the R-matrix theory by

$$b_R(E)=\sum_j\frac{i\Gamma_{jn}^0}{E-E_j+i\Gamma_j/2}, \tag{12}$$

where the summation j is carried out over all resonances. The resonances are described [29] by the resonance energy E_j, the total width Γ_j, and the reduced neutron width Γ_{jn}^0. The scattering length Eq. (12) includes the zero-energy contribution $b_R(0)$ which is a part of the nucleus coherent scattering length $b_c(E)$. Because of this we have to consider for the resonance correction only $b_R(E)$-$b_R(0)$.

D. Condensed matter effects

The correction for the interference effects in liquids was introduced by Eq. (4) using the functions $S_{\rm coh}(E)$ and $S_{\rm inc}(E)$. These functions were derived by Placzek *et al.* [32,33] in the 1950s and are shown in the relations Eqs. (13), (14):

$$S_{\rm coh}(E)=\left(\frac{m_A}{m_A+m_n}\right)^2\left(1+\frac{k_B\theta}{2m_AE}-\frac{C(\theta,E)}{E}\right), \tag{13}$$

$$S_{\rm inc}(E)=\left(\frac{m_A}{m_A+m_n}\right)^2\left(1+\frac{k_B\theta}{2m_AE}\right), \tag{14}$$

where k_B is the Boltzmann constant and θ the sample temperature. The quantity $k_B\theta/(2m_AE)$ gives the Doppler term and accounts for dynamic effects in the liquid. The term $C(\theta,E)$ in Eq. (13) comes from effects of the static structure of the liquid.

Previously in Ref. [4] we assumed that $C(\theta,E)$ is given by $C(\theta)$ of the following Eq. (15) which does not depend on the neutron energy E:

$$C(\theta)=\frac{h^2\rho_L^{2/3}}{16\pi m_n}\int_0^\infty[1-S(\mathbf{q})]\frac{d\mathbf{q}}{q}, \tag{15}$$

where ρ_L is the density and $S(\mathbf{q})$ is the static structure function as it has been derived for a hard sphere model [34]. The energy dependence is removed by the integration with the asymptotic limit, where the **q**-integration is extended over a sphere with an infinite radius. Also in the work of Melkonian *et al.* [5] the correction was made with $C(\theta)$ of Eq. (15).

At neutron energies as low as 0.1 eV this asymptotic limit is no longer adequate. Therefore we integrated only up to a

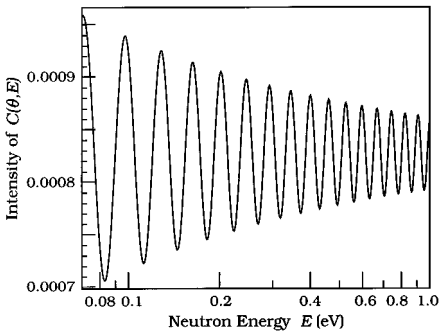

FIG. 6. Plot of $C(\theta,E)$ for liquid lead.

sphere of the radius $2k_0$ where k_0 is the wave number of the incoming neutron. An energy dependency is obtained for $C(\theta,E)$ in Eq. (16) by

$$C(\theta,E)=\frac{h^2\rho_L^{2/3}}{16\pi m_n}\int_0^{2k_0}[1-S(\mathbf{q})]\,\frac{d\mathbf{q}}{q}. \tag{16}$$

The numerical integration over the static structure function is actually only necessary for neutron energies below $\simeq 0.5$ eV; at higher energies the asymptotic function is sufficient. To derive this integral we used the static structure function as described by Ashcroft and Lekner [35], i.e., the solution of a hardcore model. In Fig. 6 the energy dependence of the term $C(\theta,E)$ is plotted for liquid lead at a temperature of 623 K.

E. Static structure functions

As mentioned in the previous section we have used a hard-core model for the static structure function, and although this model is rather simple it can accurately describe this function for liquid lead. The calculated function by Dahlborg *et al.* [34] is compared to experimental data in Fig. 7. In spite of this good agreement the uncertainty in the determination of the liquid density and the hard core diameter leads to a relative large systematic uncertainty for determining the neutron-electron scattering length.

To estimate the size of this uncertainty we used two different approaches.

(i) As in the previous evaluation [4], we fitted our data for different energy ranges. As the condensed matter correction decreases with increasing neutron energy, shifting the fitted

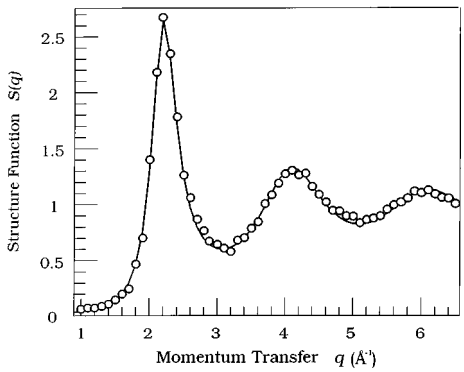

FIG. 7. Static structure function $S(q)$ for liquid lead at a temperature of 623 K.

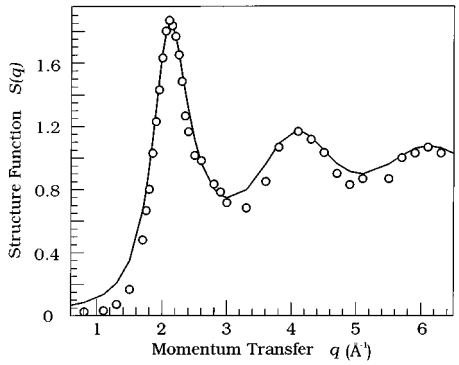

FIG. 8. Static structure function $S(q)$ for liquid bismuth.

energy range to higher energies should reduce the influence of this correction. But with higher neutron energies the effect from b_{ne} becomes smaller and increases the statistical uncertainty. Nevertheless this procedure allows us to check whether the value of b_{ne} exhibits a constant increase or decrease with increasing lower limit. Any such behavior would give a strong indication that something is wrong with the correction. The numerical details are very similar to those given in a table in Ref. [4].

(ii) In the second step, we changed the liquid parameters within their determined uncertainty leading to an estimate for the total systematic uncertainty of 0.03×10^{-3} fm. This is the only systematic uncertainty and is quoted in the final result.

Unlike that for the liquid lead sample, the static structure function of liquid bismuth cannot be described satisfactorily with the simple hard sphere model. This is due to the ''shoulder'' at the first peak in the static structure function, see Fig. 8, and to the fact that the hard sphere density is not in agreement with the ''physical'' liquid density. Therefore one should bear in mind these two problems when applying the rather simple condensed matter correction and an additional systematic uncertainty should be introduced. We estimated that the systematic uncertainty should be increased by at least a factor of two and we quote a systematic uncertainty of 0.06×10^{-3} fm for bismuth.

V. RESULTS

Results were obtained for both liquid samples of ^{208}Pb and ^{209}Bi applying the evaluation procedure in Sec. IV B. The given statistical uncertainties include the additional uncertainty introduced by the uncertainty of the free normalization parameter.

A. Neutron-TOF measurements of liquid ^{208}Pb

As decribed in Ref. [4] all eight runs were corrected separately for deadtime, overlap, and background. Averaging these runs gave the transmission values and statistical uncertainties as listed in Table II and plotted in Fig. 9. Small differences between Table II and Fig. 9 occur and are caused by averaging over different energy intervals.

The final result for the neutron-electron scattering length b_{ne} is $(-1.331\pm0.027)\times10^{-3}$ fm. As quoted throughout this article, all statistical uncertainties correspond to a one standard deviation (σ). Figure 9 indicates the positive and

TABLE II. Transmission $T(E)$ of 5 cm thorogenic liquid ^{208}Pb for the weighted mean of all eight runs as a function of the neutron energy E.

E(eV)	$T(E)$	E(eV)	$T(E)$
0.0892	0.17924(9)	5.6014	0.17364(14)
0.1097	0.17858(8)	6.8897	0.17386(14)
0.1349	0.17824(8)	8.4741	0.17384(15)
0.1660	0.17752(8)	10.4230	0.17346(15)
0.2041	0.17699(8)	12.8200	0.17348(16)
0.2511	0.17679(9)	15.7683	0.17357(16)
0.3088	0.17615(9)	19.3947	0.17354(17)
0.3799	0.17587(9)	23.8550	0.17368(18)
0.4672	0.17552(9)	29.3411	0.17329(18)
0.5747	0.17540(10)	36.0889	0.17326(19)
0.7069	0.17518(10)	44.3885	0.17334(19)
0.8694	0.17483(10)	54.5968	0.17305(20)
1.0694	0.17471(11)	67.1529	0.17305(20)
1.3153	0.17447(11)	82.5965	0.17370(21)
1.6178	0.17435(11)	101.5918	0.17306(22)
1.9898	0.17418(12)	124.9555	0.17353(23)
2.4474	0.17438(12)	153.6924	0.17358(23)
3.0103	0.17415(13)	189.0382	0.17283(24)
3.7026	0.17360(13)	232.5126	0.17298(25)
4.5541	0.17386(14)	285.9852	0.17319(26)

negative σ deviation from the solid fit curve by two dashed lines. The small change with respect to the previously reported value [4] is within experimental uncertainties and arises from the new condensed matter correction explained by Eq. (16). Also, a very small shift of the result occurs because of taking now a much broader energy range from 0.08 to 800 eV.

Including the systematic uncertainty as discussed in Sec. IV D, our new value for b_{ne} is given in Eq. (17) by

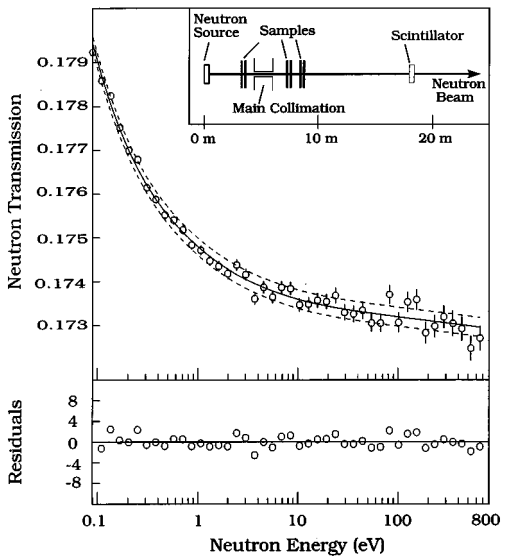

FIG. 9. Neutron transmission data of 5 cm thorogenic liquid ^{208}Pb and the final fit to obtain b_{ne}. The insert shows the neutron-TOF arrangement at 18 m, flight path No. 1.

TABLE III. Results for b_{ne} in units of 10^{-3} fm for the ^{209}Bi data for energies of a crystal spectrometer at 0.10, 0.28, 1.00, and 4.00 eV.

b_{ne}	χ^2 per degree of freedom
-1.576 ± 0.067	0.72
-1.480 ± 0.095	1.37
-1.373 ± 0.091	0.86
-1.388 ± 0.084	1.04
-1.263 ± 0.095	0.96
-1.439 ± 0.038	average value

$b_{ne}=(-1.331\pm0.027\pm0.03)\times10^{-3}$ fm where the statistical and the systematic uncertainties are denoted.

B. Melkonian's data for liquid ^{209}Bi

As already shown in Table I the original result of Melkonian *et al.* [5] was $b_{ne}=(-1.56\pm0.05)\times10^{-3}$ fm. Later Koester *et al.* [15] obtained a smaller negative value of $b_{ne}=(-1.49\pm0.05)\times10^{-3}$ fm by correcting for the Schwinger scattering. In this work we evaluated separately all ten data sets of Melkonian and obtained the results shown in the Tables III and IV. Taking the weighted mean values of the b_{ne} values of Tables III and IV and the systematic uncertainty from Sec. IV D, we obtained for the neutron-electron scattering length $b_{ne}=(-1.438\pm0.033\pm0.06)\times10^{-3}$ fm where the statistical and the systematic uncertainties are quoted.

For completeness we would like to mention the good agreement we obtained for the two data sets shown in Fig. 2. We obtained the values $b_{ne}=(-1.373\pm0.091)\times10^{-3}$ fm for liquid ^{209}Bi and $b_{ne}=(-1.361\pm0.069)\times10^{-3}$ fm for liquid ^{208}Pb. But since Fig. 2 covers only a small fraction of total running times, we hope to get some more conclusive information by a comparison between the two final results in Eq. (17) and Eq. (18) in the next section.

VI. CONCLUSION

A. Comparison between ^{208}Pb data and ^{209}Bi data

Based on the surprising agreement between ^{208}Pb data and ^{209}Bi data for single data sets as shown in Fig. 2, we decided to study [6] the reason for the discrepant results as shown in Table I. Parallel to this the new solid state correction given by Eq. (16) was developed and applied to the

TABLE IV. Results for b_{ne} in units of 10^{-3} fm for the ^{209}Bi data for energies of a crystal spectrometer at 0.10, 0.28, and 1.00 eV.

b_{ne}	χ^2 per degree of freedom
-1.692 ± 0.133	0.41
-1.517 ± 0.167	2.65
-1.223 ± 0.140	0.28
-1.478 ± 0.173	1.72
-1.199 ± 0.168	1.60
-1.434 ± 0.068	average value

computer code for a better evaluation. This led finally to the results for ^{208}Pb data shown in Eq. (17) and for ^{209}Bi data given in Eq. (18)

$$b_{ne} = (-1.33 \pm 0.027 \pm 0.03) \times 10^{-3} \text{ fm}, \quad (17)$$

$$b_{ne} = (-1.44 \pm 0.033 \pm 0.06) \times 10^{-3} \text{ fm}, \quad (18)$$

where in both equations the two uncertainties denote the statistical and the systematic uncertainty, respectively.

Considering only statistical uncertainties the difference between the related b_{ne} values is about 2.6 σ. Including the systematic uncertainties, the b_{ne} values of Eqs. (17) and (18) are fully compatible. The basis for this is the discussion of systematic uncertainties in Sec. IV D, where uncertainties of the static structure function of $S(q)$ were transformed to uncertainties for the b_{ne} values. However, even with smaller systematic uncertainties the results would still be compatible.

Considering the value of Eq. (18) with respect to the literature in Table I, we see that the result is in the middle between the Garching-Argonne and Dubna values. The answer to the question is still open, whether the less well known liquid correction of Bi or problems by the sample preparation mentioned by the authors [5] is more important.

B. Neutron-TOF measurements of liquid ^{208}Pb

The new result of b_{ne} Eq. (17) is slightly more negative than our previous value [4] from the new liquid matter correction, where by the control of the static structure function, a higher systematic accuracy is possible.

The present type of investigation is so far the only accurate method where b_{ne} is determined in a measurement with one experimental setup geometry. The result is in good agreement with the Garching-Argonne result, but in disagreement with the Dubna value, see Table I. Finally, with the agreement of ^{208}Pb data and ^{209}Bi data we obtain an important confirmation of our result.

Future experiments of this type look very encouraging and improvements are expected. Because of the surprising low background [4], measurements with thicker samples seem to be feasible which have higher sensitivities for b_{ne}, see Eq. (3). A much higher accuracy might be possible by replacing the rather slow ^{6}Li scintillator (with a considerable amount of late light) with a future development of the very attractive liquid ^{3}He scintillator.

ACKNOWLEDGMENTS

We thank the ORELA staff for providing us with excellent experimental conditions. We thank also H. Leeb, D. C. Larson, and H. Rauch for their interest and support. Oak Ridge National Laboratory is managed by Lockheed Martin Energy Research Corp. for the U.S. Department of Energy under Contract No. DE-AC05-96-OR22464. This research was supported by the Austrian Fonds zur Förderung der Wissenschaftlichen Forschung under P-9802.

[1] V. F. Sears, Phys. Rep. **141**, 281 (1986).
[2] D. E. Cullen *et al.*, Report No. UCRL-50400, 1989 (unpublished), Vol. 6.
[3] L. Koester, W. Waschkowski, L. V. Mitsyna, G. S. Samosvat, P. Prokofjevs, and J. Tambergs, Phys. Rev. C **51**, 3363 (1995).
[4] S. Kopecky, P. Riehs, J. A. Harvey, and N. W. Hill, Phys. Rev. Lett. **74**, 2427 (1995); S. Kopecky, J. A. Harvey, N. W. Hill, P. Riehs, and J. Schmiedmayer, *Baryons '92* (Yale University Press, New Haven, 1992), p. 48.
[5] E. Melkonian, B. M. Rustad, and W. W. Havens, Jr., Phys. Rev. **114**, 1571 (1959).
[6] M. Krenn, Ph.D. thesis, TU-Vienna, 1995.
[7] E. Fermi and L. Marshall, Phys. Rev. **72**, 1139 (1947).
[8] W. W. Havens, Jr., L. J. Rainwater, and I. I. Rabi, Phys. Rev. **82**, 345 (1951).
[9] M. Hamermesh, G. R. Ringo, and A. Wattenberg, Phys. Rev. **85**, 483 (1952).
[10] D. J. Hughes, J. A. Harvey, M. D. Goldberg, and Marilyn J. Stafne, Phys. Rev. **90**, 497 (1953).
[11] M. F. Crouch, V. E. Krohn, and G. R. Ringo, Phys. Rev. **102**, 1321 (1956).
[12] V. E. Krohn and R. G. Ringo, Phys. Rev. **148**, 1303 (1966).
[13] V. E. Krohn and R. G. Ringo, Phys. Rev. D **8**, 1305 (1973).
[14] Yu. A. Alexandrov, T. A. Machekhina, L. N. Sedlakova, and L. E. Fykin, Sov. J. Nucl. Phys. **20**, 623 (1975).
[15] L. Koester, W. Nistler, and W. Waschkowski, Phys. Rev. Lett. **36**, 1021 (1976).
[16] Yu. A. Alexandrov, M. Vrana, Garcia J. Manrique, T. A. Machekhina, and L. N. Sedlakova, Sov. J. Nucl. Phys. **44**, 900 (1986).
[17] L. Koester, W. Waschkowski, and A. Klüver, Physica B **137**, 282 (1986).
[18] L. L. Foldy, Phys. Rev. **87**, 688 (1952).
[19] Yu. A. Alexandrov, Nucl. Instrum. Methods Phys. Res. A **284**, 134 (1989).
[20] V. G. Nikolenko and A. B. Popov, Z. Phys. A **341**, 365 (1992).
[21] Yu. A. Alexandrov, Z. Phys. A **344**, 219 (1992).
[22] H. Leeb and C. Teichtmeister, Phys. Rev. C **48**, 1719 (1993).
[23] Yu. A. Alexandrov, Phys. Rev. C **49**, R2297 (1994), and references therein.
[24] Yu. A. Alexandrov, Neutron News **5** (1), 20 (1994); **5** (4), 17 (1994).
[25] J. Byrne, Neutron News **5** (4), 15 1994.
[26] A. W. Thomas, S. Theberge, and Gerald A. Miller, Phys. Rev. D **24**, 216 (1981).
[27] A. Ioffe, M. Vrana, and V. Zabiyakin, *Proceedings of the International Symposium on Neutron Optics and Related Research Facilities*, Kumatori, 1996, [J. Phys. Soc. Jpn. **65**, 90 (1996)].
[28] G. G. Bunatian, V. G. Nikonenko, A. B. Popov, G. S. Samos-

vat, and T. Yu. Tretiakova, Dubna Report No. E3-96-79, 1996 (unpublished).
[29] S. F. Mughabghab, M. Divadeenam, and N. E. Holden, *Neutron Cross Sections* (Academic, New York, 1984), Vol. 1, Pt. B.
[30] L. Koester, H. Rauch, and E. Seymann, At. Data Nucl. Data Tables **49**, 65 (1991).
[31] J. Schmiedmayer, P. Riehs, J. A. Harvey, and N. W. Hill, Phys. Rev. Lett. **66**, 1015 (1991), and references therein.
[32] G. Placzek, B. R. A. Nijboer, and L. Van Hove, Phys. Rev. **82**, 392 (1951).
[33] J. R. Granada, Z. Naturforsch. Teil A **39**, 1160 (1984).
[34] U. Dahlborg, M. Davidovic, and K.E. Larsson, Phys. Chem. Liq. **6**, 149 (1977).
[35] N. W. Ashcroft and J. Lekner, Phys. Rev. **145**, 83 (1966).